

University of Massachusetts Medical School

eScholarship@UMMS

---

Open Access Articles

Open Access Publications by UMMS Authors

---

2020-05-07

## Neuroigin3 splice isoforms shape inhibitory synaptic function in the mouse hippocampus


Motokazu Uchigashima

*University of Massachusetts Medical School*

*Et al.*

Let us know how access to this document benefits you.

Follow this and additional works at: <https://escholarship.umassmed.edu/oapubs>

 Part of the [Amino Acids, Peptides, and Proteins Commons](#), [Cell Biology Commons](#), [Developmental Neuroscience Commons](#), [Molecular and Cellular Neuroscience Commons](#), [Molecular Biology Commons](#), [Nervous System Commons](#), and the [Nucleic Acids, Nucleotides, and Nucleosides Commons](#)

---

### Repository Citation

Uchigashima M, Leung M, Watanabe T, Cheung A, Le T, Pallat S, Marques Dinis AL, Watanabe M, Imamura Kawasawa Y, Futai K. (2020). Neuroigin3 splice isoforms shape inhibitory synaptic function in the mouse hippocampus. Open Access Articles. <https://doi.org/10.1074/jbc.AC120.012571>. Retrieved from <https://escholarship.umassmed.edu/oapubs/4247>

This material is brought to you by eScholarship@UMMS. It has been accepted for inclusion in Open Access Articles by an authorized administrator of eScholarship@UMMS. For more information, please contact [Lisa.Palmer@umassmed.edu](mailto:Lisa.Palmer@umassmed.edu).

## Neurologin3 splice isoforms shape inhibitory synaptic function in the mouse hippocampus

Motokazu Uchigashima<sup>1,2,5</sup>, Ming Leung<sup>3,5</sup>, Takuya Watanabe<sup>1,5</sup>, Amy Cheung<sup>1</sup>, Timmy Le<sup>1</sup>, Sabine Pallat<sup>1</sup>, Alexandre Luis Marques Dinis<sup>1</sup>, Masahiko Watanabe<sup>2</sup>, Yuka Imamura Kawasawa<sup>3,4\*</sup> and Kensuke Futai<sup>1\*</sup>

<sup>1</sup>Brudnick Neuropsychiatric Research Institute, Department of Neurobiology, University of Massachusetts Medical School, 364 Plantation Street, LRB-706 Worcester, MA 01605-2324, USA

<sup>2</sup>Department of Anatomy, Hokkaido University Graduate School of Medicine, Sapporo, Hokkaido 060-8638, Japan

<sup>3</sup>Department of Biochemistry and Molecular Biology and Institute for Personalized Medicine, Pennsylvania State University College of Medicine, 500 University Drive, Hershey, Pennsylvania 17033, USA

<sup>4</sup>Department of Pharmacology Pennsylvania State University College of Medicine, 500 University Drive, Hershey, Pennsylvania 17033, USA

<sup>5</sup>These authors contributed equally

\*Corresponding authors:

Yuka Imamura Kawasawa

E-mail: [yimamura@pennstatehealth.psu.edu](mailto:yimamura@pennstatehealth.psu.edu)

Kensuke Futai

E-mail: [Kensuke.Futai@umassmed.edu](mailto:Kensuke.Futai@umassmed.edu)

**Running title:** NLGN3 expression and function in mouse hippocampal neurons

### KEYWORDS

Neurobiology, neuron, trans-synaptic cell adhesion, neurotransmitter receptor, GABA receptor, glutamate receptor, excitatory and inhibitory balance, hippocampus, CA1 pyramidal neuron, splice variants, neurologin 3 (NLGN3), synaptic transmission

## Abstract

**Synapse formation is a dynamic process essential for the development and maturation of the neuronal circuitry in the brain. At the synaptic cleft, trans-synaptic protein–protein interactions are major biological determinants of proper synapse efficacy. The balance of excitatory and inhibitory synaptic transmission (E-I balance) stabilizes synaptic activity, and dysregulation of the E-I balance has been implicated in neurodevelopmental disorders, including autism spectrum disorders. However, the molecular mechanisms underlying the E-I balance remain to be elucidated. Here, using single-cell transcriptomics, immunohistochemistry and electrophysiology approaches to murine CA1 pyramidal neurons obtained from organotypic hippocampal slice cultures, we investigate Neuroligin (*Nlgn*) genes that encode a family of postsynaptic adhesion molecules known to shape excitatory and inhibitory synaptic function. We demonstrate that the NLGN3 protein differentially regulates inhibitory synaptic transmission in a splice isoform–dependent manner at hippocampal CA1 synapses. We also found that distinct subcellular localizations of the NLGN3 isoforms contribute to the functional differences observed among these isoforms. Finally, results from single-cell RNA-Seq analyses revealed that *Nlgn1* and *Nlgn3* are the major murine *Nlgn* genes and that the expression levels of the *Nlgn* splice isoforms are highly diverse in CA1 pyramidal neurons. Our results delineate isoform-specific effects of *Nlgn* genes on the E-I balance in the murine hippocampus.**

## Introduction

Neuroligin proteins (NLGNs) were the first identified binding partners of  $\alpha$ -latrotoxin receptors, neurexin proteins (NRX), and localize at postsynaptic sites to regulate synapse maturation and function (1). Four *Nlgn* genes (*Nlgn1*, *Nlgn2*, *Nlgn3* and *Nlgn4*) encode trans-synaptic adhesion proteins (NLGN1, NLGN2, NLGN3 and NLGN4) that contain extracellular cholinesterase-like domains and transmembrane and PDZ-binding motif-containing intracellular domains. While the intracellular domain is important for NLGN binding

with postsynaptic scaffold molecules, the extracellular domain confers the formation of excitatory and inhibitory synapses with NRX, its sole presynaptic binding partner. Therefore, precise combinations of NRX-NLGN interactions allow NLGN to diversify synapse identity.

NLGN1 and NLGN2 are postsynaptic adhesion molecules localized to excitatory and inhibitory synapses, respectively. Overexpression, knockdown and knockout approaches have revealed that NLGN1 is important for excitatory synaptic structure and transmission and synaptic plasticity, but not for inhibitory synaptic function (2-6). NLGN2 protein has specific functional roles in inhibitory synaptic transmission in the hippocampus (6-8). In contrast, it has been reported that NLGN3 protein localizes at both excitatory and inhibitory synaptic sites and regulates both synaptic functions (7-12). This unique ability alludes to a NLGN3 protein-specific molecular code that promotes its translocation to both excitatory and inhibitory sites.

Splice insertion in *Nlgn* genes differentially regulates E-I balance and alters their binding affinity with presynaptic NRX proteins. In the extracellular cholinesterase-like domain, *Nlgn* genes have one or two splice insertion sites, *Nlgn1* (A and B sites), *Nlgn2* (A) and *Nlgn3* (A1 and A2), leading to two to four theoretical splice isoforms. The splice insertion site B in NLGN1 determines its binding preference to NRXs (13,14) and excitatory synaptic function (15). Similarly, NLGN2 contains a splice insertion at site A which regulates inhibitory synaptic function (8). However, to the best of our knowledge, the splice isoform-specific function of NLGN3 and the transcript levels of *Nlgn* splice isoforms at the single-cell level have not been addressed.

In the present study, we assess the function of NLGN3 splice isoforms on excitatory and inhibitory synaptic transmission in CA1 pyramidal neurons in mouse organotypic slice cultures. Our results suggest that NLGN3 up- or down- regulates inhibitory synaptic transmission in a splice isoform-dependent manner. Furthermore, our single-cell RNA sequencing (RNA-seq) analysis reveals that *Nlgn1* and *Nlgn3* are the major *Nlgn* genes and the expression of *Nlgn* splice variants are highly distinct in hippocampal CA1 pyramidal neurons.

## Results

## NLGN3 splice isoform-dependent regulation of inhibitory synaptic transmission

The *Nlgn3* gene contains two splice insertion sites (A1 and A2) that can yield four NLGN3 splice isoforms (NLGN3 $\Delta$ , A1, A2 and A1A2). NLGN3 $\Delta$  lacks all splice insertions, while NLGN3A1, 3A2 and 3A1A2 receive insertion of A1, A2 or both A1A2 cassette(s), respectively. To examine the potential roles of NLGN3 splice isoforms on excitatory and inhibitory synapse function, we biolistically transfected the *Nlgn3* splice isoform genes in CA1 pyramidal cells of organotypic hippocampal slice cultures (**Fig. 1**). Transfection of NLGN3 splice variants did not alter gross cell morphology or levels of overexpressed NLGN3 splice variants identified by HA immunoreactivity (**Fig. S1A**). Simultaneous electrophysiological recordings were made from transfected and neighboring untransfected neurons. CA1 pyramidal neurons overexpressing NLGN3 $\Delta$  or 3A2 showed increased evoked IPSCs compared with neighboring untransfected control neurons and a marked increase in EPSCs, as reported previously (**Fig. 1A and C**) (7,12). In contrast, overexpression of NLGN3A1 or 3A1A2 resulted in reduced amplitude of IPSCs and increased amplitude of EPSCs compared with neighboring untransfected cells (**Fig. 1B and D**). Paired stimulation of input fibers with short interval (50 ms) induced paired-pulse facilitation (PPF) and depression (PPD) of EPSCs and IPSCs, respectively. NLGN3 $\Delta$  or 3A2 transfection displayed both reduced AMPAR-PPF and GABA<sub>A</sub>R-PPD compared with untransfected neurons, consistent with previous work (5,7) (**Fig. S1D and E**). As paired-pulse ratio (PPR) inversely correlates with presynaptic release probability, these results suggest that overexpression of NLGN3 $\Delta$  and 3A2 can modulate presynaptic release probability. NLGN3 increased or decreased inhibitory synaptic transmission in a splice isoform-dependent manner, whereas all NLGN3 splice isoforms enhanced excitatory synaptic transmission. Next, we tested whether NLGN3 overexpression changes membrane excitability. The input-output (I-O) relationship of CA1 pyramidal neurons transfected with NLGN3 splice isoform exhibited no significant difference compared with untransfected control neurons (**Fig. S2**). The findings above suggest that NLGN3 splice isoforms regulate synaptic but not membrane functions.

## Subcellular localization of NLGN3 splice isoforms in the dendritic segment of CA1 pyramidal neurons

Expression of NLGN3 at excitatory and inhibitory synapses has been observed in primary neurons but *in vivo* NLGN3 expression has been studied only in the cerebellum and striatum (11,16,17). To ensure the expression of NLGN3 in the hippocampus, we performed immunohistochemistry against NLGN3 with the markers for excitatory and inhibitory synapses, VGluT1 and VIAAT, respectively (**Fig. 2**). Our NLGN3 antibody, validated by *Nlgn3* knockout tissue, detected punctate signals in the hippocampus (**Fig. 2A and B**). The signals overlapped with VGluT1 and VIAAT puncta, indicating that NLGN3 proteins are targeted to both excitatory and inhibitory synapses, respectively (**Fig. 2C and D**). To understand the mechanistic roles of NLGN3 splice isoforms in inhibitory synaptic transmission, we next performed immunocytochemistry to elucidate the subcellular localization of NLGN3 $\Delta$  and 3A1A2, which displayed strong enhancement and suppression of IPSC, respectively. Excitatory synaptic sites were characterized by spine or VGluT1. Inhibitory synaptic sites were identified by the dendritic shaft proximal to VIAAT puncta. HA immunoreactivity illustrated that NLGN3A1A2 is highly concentrated in spines. In contrast, NLGN3 $\Delta$  showed more diffuse expression in both spines and dendrites (**Fig. 3A**). The ratio of NLGN3A1A2 signals between excitatory and inhibitory synapses was significantly higher than that of 3 $\Delta$  (**Fig. 3B**). Next, we addressed whether these NLGN3 splice isoforms differentially promote excitatory and inhibitory synapses by comparing NLGN3/GFP and GFP (control) transfected neurons. Importantly, inhibitory synapse density was comparable among NLGN3 $\Delta$ , 3A1A2 and control, whereas VIAAT signal intensity in 3 $\Delta$ -expressing neurons was significantly higher than that of 3A1A2 and control (**Fig. 3C and D**). The spine density or length was comparable among NLGN3 $\Delta$ , 3A1A2 and control neurons (**Fig. 3E and F**). The signal intensities of VGluT1 were markedly elevated in neurons overexpressing NLGN3 $\Delta$  or 3A1A2 compared with control neurons (**Fig. 3G and H**). These results suggest that differences in the subcellular localization of NLGN3 $\Delta$  and 3A1A2 contribute to their distinct inhibitory synaptic functions. Lastly, we tested whether NLGN3 $\Delta$  or 3A1A2 overexpression changes endogenous expression of NLGN2 protein, an inhibitory synapse-specific NLGN protein (3,18). Immunohistochemistry against GFP, VIAAT and NLGN2 revealed that transfection of NLGN3 splice isoform has no effect on the level of

endogenous NLGN2 at inhibitory synapses (**Fig. S3**). This result suggests that the physiological and anatomical phenotypes we observed in **Fig. 1 and 3** are mediated by overexpressed NLGN3 and not due to an indirect detrimental side effect of transgene overexpression.

### Endogenous expression of *Nlgn* genes and splice isoforms in hippocampal CA1 pyramidal neurons

Finally, to understand the expression of endogenous *Nlgn* genes in CA1 pyramidal neurons, we harvested cytosol from four neurons and performed single-cell deep RNA-seq. The t-SNE plot indicates that the four cell transcripts (G418) were clustered together and close to that of adult hippocampal CA1-3 pyramidal neurons derived from the Allen Brain Atlas (**Fig. 4A**). The expression of *Nlgn* genes was clustered and well correlated with the single-cell RNA-seq data in the RNA-seq datasets provided by the Allen Institute for Brain Science (**Fig. 4B**). The quantification of *Nlgn* genes (**Fig. 4C**) indicates that the expression of *Nlgn1* and *Nlgn3* are comparable but that of *Nlgn2* is significantly lower than the other two genes. We also compared the expression of *Nlgn* splice isoforms in each *Nlgn* gene. Six *Nlgn* splice isoforms, *Nlgn1A*, *1B*, *2A*, *3A* and *3A1*, that were not annotated, were manually modified (**Fig. S4A**), and their expression was compared. *Nlgn1A*, *1B* and *1AB* were the most highly expressed *Nlgn1* splice isoforms (**Fig. 4D**). *Nlgn2A* was the only isoform counted in the *Nlgn2* gene (**Fig. 4E**). *Nlgn1A* and *2A* transcripts were not detected in any of the four CA1 pyramidal neurons. Importantly, *Nlgn3A* and *3A2*, which exhibited increased inhibitory synaptic transmission, were the dominant *Nlgn3* splice isoforms in CA1 pyramidal neurons (**Fig. 4F**). The expression of *Nlgn3A1* and *3A1A2* were significantly lower than *Nlgn3A* (TPM: *Nlgn3A1*:  $0.004 \pm 0.004$ , *3A1A2*:  $0.3 \pm 0.3$ ). The expression of these single-cell *Nlgn* splice isoforms were also confirmed by semi-quantitative PCRs (**Fig. S4B**).

### Discussion

Trans-synaptic protein-protein interactions are fundamental biological events for synapse formation, maturation and function. NLGNs are critical postsynaptic adhesion molecules that regulate excitatory and inhibitory synaptic transmission. Here we demonstrated that NLGN3 regulates inhibitory synaptic transmission and excitatory and inhibitory

synapse localization in a splice isoform-dependent manner. Our single-cell transcriptome analysis revealed that *Nlgn3A* and *3A2* are the highest expressed *Nlgn3* splice isoforms in hippocampal CA1 pyramidal neurons.

The distinct subcellular localization of NLGN3 $\Delta$  and 3A1A2 suggests intriguing mechanisms regarding how splice isoforms influence synapse specificity. Given that the intracellular and transmembrane domains are identical between NLGN3 splice isoforms, each isoform exerts their synapse coding effect through their unique extracellular domains. Similarly, the extracellular domain of NLGN2 mediates changes in inhibitory synaptic function (6). Based on our current knowledge, NRXs are the only trans-synaptic family proteins that directly bind to NLGNs. Trans-synaptic interactions between NLGN3 $\Delta$ , but not 3A1A2, and NRXs modulate inhibitory synaptic transmission in pyramidal neurons. We previously reported that postsynaptic NLGN2 can couple with presynaptic  $\alpha$ NRX1 but not with  $\beta$ NRX1 to form functional inhibitory synapses (6), suggesting that the specific binding of NLGN and NRX isoforms regulates functional synapse formation. It is possible that inhibitory interneurons do not express NRX isoforms that can bind to NLGN3A1A2. Therefore, NLGN3A1A2 may exclusively localize to excitatory synapses. Further studies should be performed to identify specific NRX-NLGN3 isoform interactions which affect inhibitory synaptic function. Another possible mechanism is cis-cis protein interactions between NLGN3 and postsynaptic proteins. It has been reported that protein complexes formed between the extracellular domain of NLGN1 and NMDAR are important for synaptic function (19). NLGN3 splice variants may have different binding interactions with postsynaptic proteins which provide distinct functions on inhibitory synapses. It has been suggested that the relative levels of NLGNs and their postsynaptic scaffold complex at excitatory and inhibitory synapses determine E-I balance (20). Additional studies are required, but it is interesting to address the hypothesis that postsynaptic NLGN3A1 and A1A2 are strong and specific regulators at excitatory synaptic sites and sequester the necessary protein interactions (i.e., NLGN2-mediated scaffold complex) from inhibitory synapses to reduce inhibitory synaptic transmission.

The single-cell sequencing results demonstrate a comprehensive unbiased gene expression profile of *Nlgn* splice isoforms in hippocampal CA1 pyramidal neurons obtained from neonatal mice. Our transcriptome findings are highly correlated with the

expression pattern of the three *Nlgn*s genes provided by the Allen Brain Atlas single-cell database from adult neurons, indicating that the expression ratio of *Nlgn*s are stable throughout development. Interestingly, NLGN2 has been well-characterized at inhibitory synapses, yet its transcript levels were significantly lower than *Nlgn1* and *Nlgn3* (Fig. 4B and C). NLGN2 may have unique post-translational modifications and turnover mechanisms compared with NLGN1 and NLGN3. The expression of *Nlgn3A1* and *3A1A2* were much lower than *Nlgn3A* and *3A2*, suggesting that these two splice isoforms are not the major functional *Nlgn3* molecules under basal conditions. Further work is necessary to address whether modifications to neuronal activity such as synaptic plasticity can alter the expression of *Nlgn* splice isoforms.

A shift in E-I balance has been considered a pathophysiological hallmark of neurodevelopmental disorders and repeatedly reported in corresponding mouse models (21). Mutations and deletions of *Nlgn3* loci are associated with autism spectrum disorders (22), and mutant mice that mimic the human autism *Nlgn3* mutation exhibit E-I imbalance and abnormal synaptic plasticity (1). A closer examination of specific NLGN3 splice isoform functions will elucidate their role in producing critical molecular outcomes that may influence neuropsychiatric disease pathogenesis.

## Experimental procedures

### Animal and organotypic slice culture preparation:

All animal protocols were approved and reviewed by the Institutional Animal Care and Use Committee at the University of Massachusetts Medical School and the Hokkaido University. The *Nlgn3* KO mouse line was a gift from Dr. Tanaka (23). Organotypic hippocampal slice cultures were prepared from postnatal 6- to 7-day-old C57BL6 mice of both sexes as described previously (24).

**Single-cell sequencing and analysis:** The cytosol of four CA1 neurons were harvested using the whole-cell patch-clamp technique described previously (6). Library preparation, mRNA sequencing and data analysis were done based on our established protocol. Detailed single-cell RNA-seq procedure is described in the **Supporting Experimental Procedures**.

**Immunohistochemistry and immunocytochemistry:** Mice were transcardially perfused with 4% paraformaldehyde/0.1 M phosphate buffer. Brains were

dehydrated and embedded with paraffin. Paraffin sections (2  $\mu$ m in thickness) were generated using a sliding microtome (Leica). Prior to immunoreactions, paraffin sections were boiled with Immunosaver (Nisshin EM) for 30 min. Organotypic slice cultures transfected with NLGN3 splice isoforms were fixed with 4% PFA and 4% sucrose in 0.01 M phosphate-buffered saline (PBS). Organotypic slices were permeabilized with 0.1-0.5% Triton X-100 / PBS (PBST), followed by blocking with 10% goat serum. A mixture of primary antibodies against enhanced green fluorescent protein (EGFP: chicken, Millipore), human influenza hemagglutinin (HA; rabbit, Cell signals), NLGN2 (rabbit, (16)), NLGN3 (guinea pig, (16)), vesicular glutamate transporter type 1 (VGluT1; rabbit and guinea pig, (25)) and vesicular inhibitory amino acid transporter (VIAAT; guinea pig and goat, (26)), and a mixture of species-specific secondary antibodies conjugated with Alexa 488, 555 and 647 (Thermo Fisher) were used for immunostaining. Images were taken with a confocal microscope (FV1200, Olympus) equipped with a 60x silicone oil immersion objective (UPLSAPO 60XS) and analyzed with ImageJ software.

**Electrophysiology:** Organotypic hippocampal slice cultures were prepared from postnatal 6-7 days old mice of either sex. Neurons at DIV 4-6 were transfected using a biolistic gene gun (Bio-Rad) and were assayed 3 days after transfection (DIV 7-9) as described previously (5,6,27,28). Whole-cell voltage clamp recordings were made simultaneously from a pair of CA1 pyramidal neurons, one transfected (visualized by co-transfecting GFP) and one untransfected neighbor. GABA<sub>A</sub> receptor-mediated inhibitory postsynaptic currents (IPSCs) were evoked with a stimulating electrode placed in the stratum radiatum and measured at  $V_{\text{hold}} \pm 0$  mV. AMPAR-mediated excitatory postsynaptic currents (EPSCs) were evoked at  $V_{\text{hold}} - 70$  mV in the presence of picrotoxin (0.1 mM, Sigma). Further electrophysiological procedures are described in the **Supporting Experimental Procedures**.

**Statistical analyses:** Results are reported as mean  $\pm$  s.e.m. Mann-Whitney U-test and Student's t-test were used for two-group comparison. Statistical significance was set at  $p < 0.05$  for Student's t-test and U-test.

**DATA availability:** The accession number for the RNA-seq and processed data reported in this paper is GEO: GSE143295.

Other experimental procedures are described in the **Supporting Experimental Procedures**.

**Author contributions**

M.U., T.W., Y.I.K. and K.F. designed research; M.U., M.L., T.W., A.C., T.L., S.P., A.D., Y.I.K. and K.F. carried out experiments; M.U., M.L., T.W., Y.I.K. and K.F. analyzed data; M.U., T.W., A.C., M.W., Y.I.K. and K.F. wrote the paper.

**Acknowledgement**

This work was supported by the grants from the National Institutes of Health Grants (R01NS085215 to K.F., T32 GM107000 to A.C.), Grants-in-Aid for Scientific Research (15K06732 to M.U.). The authors thank Ms. Naoe Watanabe for skillful technical assistance. We thank Dr. Paul D. Gardner for comments on the manuscript.

**Conflict of Interest:** The authors declare no conflicts of interest in regard to this manuscript.



## References

1. Sudhof, T. C. (2017) Synaptic Neurexin Complexes: A Molecular Code for the Logic of Neural Circuits. *Cell* **171**, 745-769
2. Jiang, M., Polepalli, J., Chen, L. Y., Zhang, B., Sudhof, T. C., and Malenka, R. C. (2017) Conditional ablation of neuroligin-1 in CA1 pyramidal neurons blocks LTP by a cell-autonomous NMDA receptor-independent mechanism. *Mol Psychiatry* **22**, 375-383
3. Chubykin, A. A., Atasoy, D., Etherton, M. R., Brose, N., Kavalali, E. T., Gibson, J. R., and Sudhof, T. C. (2007) Activity-dependent validation of excitatory versus inhibitory synapses by neuroligin-1 versus neuroligin-2. *Neuron* **54**, 919-931
4. Shipman, S. L., and Nicoll, R. A. (2012) A subtype-specific function for the extracellular domain of neuroligin 1 in hippocampal LTP. *Neuron* **76**, 309-316
5. Futai, K., Kim, M. J., Hashikawa, T., Scheiffele, P., Sheng, M., and Hayashi, Y. (2007) Retrograde modulation of presynaptic release probability through signaling mediated by PSD-95-neuroligin. *Nat Neurosci* **10**, 186-195
6. Futai, K., Doty, C. D., Baek, B., Ryu, J., and Sheng, M. (2013) Specific trans-synaptic interaction with inhibitory interneuronal neurexin underlies differential ability of neuroligins to induce functional inhibitory synapses. *J Neurosci* **33**, 3612-3623
7. Shipman, S. L., Schnell, E., Hirai, T., Chen, B. S., Roche, K. W., and Nicoll, R. A. (2011) Functional dependence of neuroligin on a new non-PDZ intracellular domain. *Nat Neurosci* **14**, 718-726
8. Nguyen, Q. A., Horn, M. E., and Nicoll, R. A. (2016) Distinct roles for extracellular and intracellular domains in neuroligin function at inhibitory synapses. *eLife* **5**
9. Etherton, M., Foldy, C., Sharma, M., Tabuchi, K., Liu, X., Shamloo, M., Malenka, R. C., and Sudhof, T. C. (2011) Autism-linked neuroligin-3 R451C mutation differentially alters hippocampal and cortical synaptic function. *Proc Natl Acad Sci U S A* **108**, 13764-13769
10. Foldy, C., Malenka, R. C., and Sudhof, T. C. (2013) Autism-associated neuroligin-3 mutations commonly disrupt tonic endocannabinoid signaling. *Neuron* **78**, 498-509
11. Budreck, E. C., and Scheiffele, P. (2007) Neuroligin-3 is a neuronal adhesion protein at GABAergic and glutamatergic synapses. *Eur J Neurosci* **26**, 1738-1748
12. Shipman, S. L., and Nicoll, R. A. (2012) Dimerization of postsynaptic neuroligin drives synaptic assembly via transsynaptic clustering of neurexin. *Proc Natl Acad Sci U S A* **109**, 19432-19437
13. Ichtchenko, K., Hata, Y., Nguyen, T., Ullrich, B., Missler, M., Moomaw, C., and Sudhof, T. C. (1995) Neuroligin 1: a splice site-specific ligand for beta-neurexins. *Cell* **81**, 435-443
14. Boucard, A. A., Chubykin, A. A., Comoletti, D., Taylor, P., and Sudhof, T. C. (2005) A splice code for trans-synaptic cell adhesion mediated by binding of neuroligin 1 to alpha- and beta-neurexins. *Neuron* **48**, 229-236
15. Chih, B., Gollan, L., and Scheiffele, P. (2006) Alternative splicing controls selective trans-synaptic interactions of the neuroligin-neurexin complex. *Neuron* **51**, 171-178
16. Uchigashima, M., Ohtsuka, T., Kobayashi, K., and Watanabe, M. (2016) Dopamine synapse is a neuroligin-2-mediated contact between dopaminergic presynaptic and GABAergic postsynaptic structures. *Proc Natl Acad Sci U S A* **113**, 4206-4211
17. Baudouin, S. J., Gaudias, J., Gerharz, S., Hatstatt, L., Zhou, K., Punnakkal, P., Tanaka, K. F., Spooren, W., Hen, R., De Zeeuw, C. I., Vogt, K., and Scheiffele, P. (2012) Shared synaptic pathophysiology in syndromic and nonsyndromic rodent models of autism. *Science* **338**, 128-132
18. Varoqueaux, F., Jamain, S., and Brose, N. (2004) Neuroligin 2 is exclusively localized to inhibitory synapses. *Eur J Cell Biol* **83**, 449-456
19. Budreck, E. C., Kwon, O. B., Jung, J. H., Baudouin, S., Thommen, A., Kim, H. S., Fukazawa, Y., Harada, H., Tabuchi, K., Shigemoto, R., Scheiffele, P., and Kim, J. H. (2013) Neuroligin-1 controls synaptic abundance of NMDA-type glutamate receptors through extracellular coupling. *Proc Natl Acad Sci U S A* **110**, 725-730

20. Levinson, J. N., and El-Husseini, A. (2005) Building excitatory and inhibitory synapses: balancing neuroligin partnerships. *Neuron* **48**, 171-174
21. Nelson, S. B., and Valakh, V. (2015) Excitatory/Inhibitory Balance and Circuit Homeostasis in Autism Spectrum Disorders. *Neuron* **87**, 684-698
22. Jamain, S., Quach, H., Betancur, C., Rastam, M., Colineaux, C., Gillberg, I. C., Soderstrom, H., Giros, B., Leboyer, M., Gillberg, C., and Bourgeron, T. (2003) Mutations of the X-linked genes encoding neuroligins NLGN3 and NLGN4 are associated with autism. *Nat Genet* **34**, 27-29
23. Tanaka, K. F., Ahmari, S. E., Leonardo, E. D., Richardson-Jones, J. W., Budreck, E. C., Scheiffele, P., Sugio, S., Inamura, N., Ikenaka, K., and Hen, R. (2010) Flexible Accelerated STOP Tetracycline Operator-knockin (FAST): a versatile and efficient new gene modulating system. *Biol Psychiatry* **67**, 770-773
24. Stoppini, L., Buchs, P. A., and Muller, D. (1991) A simple method for organotypic cultures of nervous tissue. *J Neurosci Methods* **37**, 173-182
25. Kawamura, Y., Fukaya, M., Maejima, T., Yoshida, T., Miura, E., Watanabe, M., Ohno-Shosaku, T., and Kano, M. (2006) The CB1 cannabinoid receptor is the major cannabinoid receptor at excitatory presynaptic sites in the hippocampus and cerebellum. *J Neurosci* **26**, 2991-3001
26. Miyazaki, T., Fukaya, M., Shimizu, H., and Watanabe, M. (2003) Subtype switching of vesicular glutamate transporters at parallel fibre-Purkinje cell synapses in developing mouse cerebellum. *Eur J Neurosci* **17**, 2563-2572
27. Hasegawa, Y., Mao, W., Saha, S., Gunner, G., Kolpakova, J., Martin, G. E., and Futai, K. (2017) Luciferase shRNA Presents off-Target Effects on Voltage-Gated Ion Channels in Mouse Hippocampal Pyramidal Neurons. *eNeuro* **4**
28. Mao, W., Salzberg, A. C., Uchigashima, M., Hasegawa, Y., Hock, H., Watanabe, M., Akbarian, S., Kawasawa, Y. I., and Futai, K. (2018) Activity-Induced Regulation of Synaptic Strength through the Chromatin Reader L3mbtl1. *Cell Rep* **23**, 3209-3222
29. van der Maaten, L., and Hinton, G. (2008) Visualizing Data using t-SNE. *J Machine Learning Research* **9**, 2579-2605
30. Bray, N. L., Pimentel, H., Melsted, P., and Pachter, L. (2016) Near-optimal probabilistic RNA-seq quantification. *Nature biotechnology* **34**, 525-527

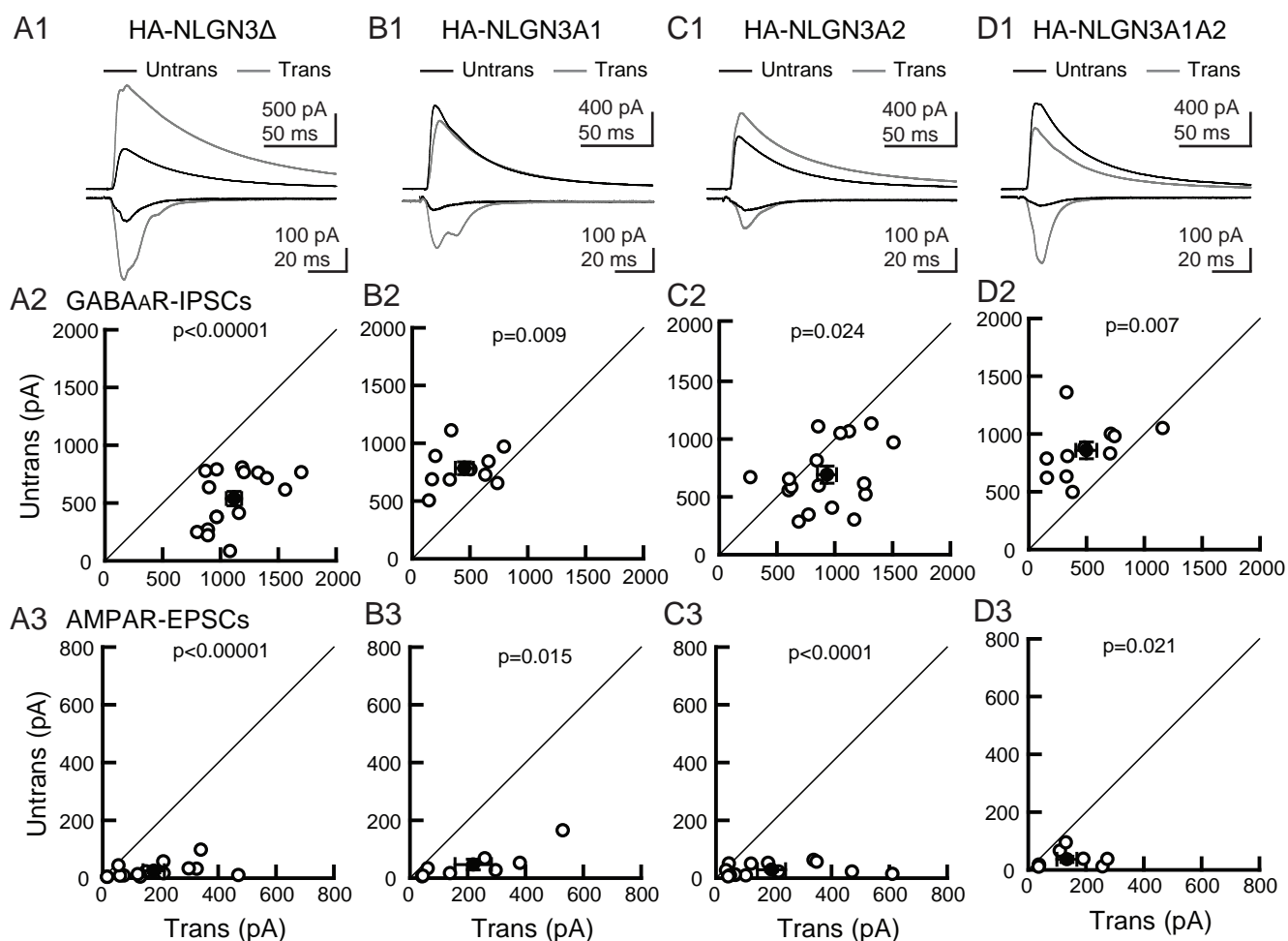


**Figure 1.** NLGN3 splice isoforms differentially encode synapse specificity. Effect of NLGN3 splice isoform overexpression on GABAAR-IPSCs and AMPAR-EPSCs in hippocampal CA1 pyramidal cells. **A1-D1.** Top row: superimposed sample IPSCs and EPSCs from pairs of transfected (gray) and untransfected (black) cells. Stimulus artifacts were truncated. **A.** NLGN3 $\Delta$ . **B.** 3A1. **C.** 3A2. **D.** 3A1A2. IPSC (middle row, **A2-D2**) and EPSC (bottom row, **A3-D3**) amplitudes were plotted for each pair of transfected (Trans) and neighboring untransfected (Untrans) cells (open symbols). Filled symbols indicate the mean  $\pm$  s.e.m. Numbers of cell pairs: NLGN3 $\Delta$  (IPSCs/EPSCs: 16/14); 3A1 (10/8); 3A2 (16/14); 3A1A2 (11/8). Number of tested slice cultures are the same as that of cell pairs. Results in all figures are reported as mean  $\pm$  s.e.m. Mann-Whitney U test.

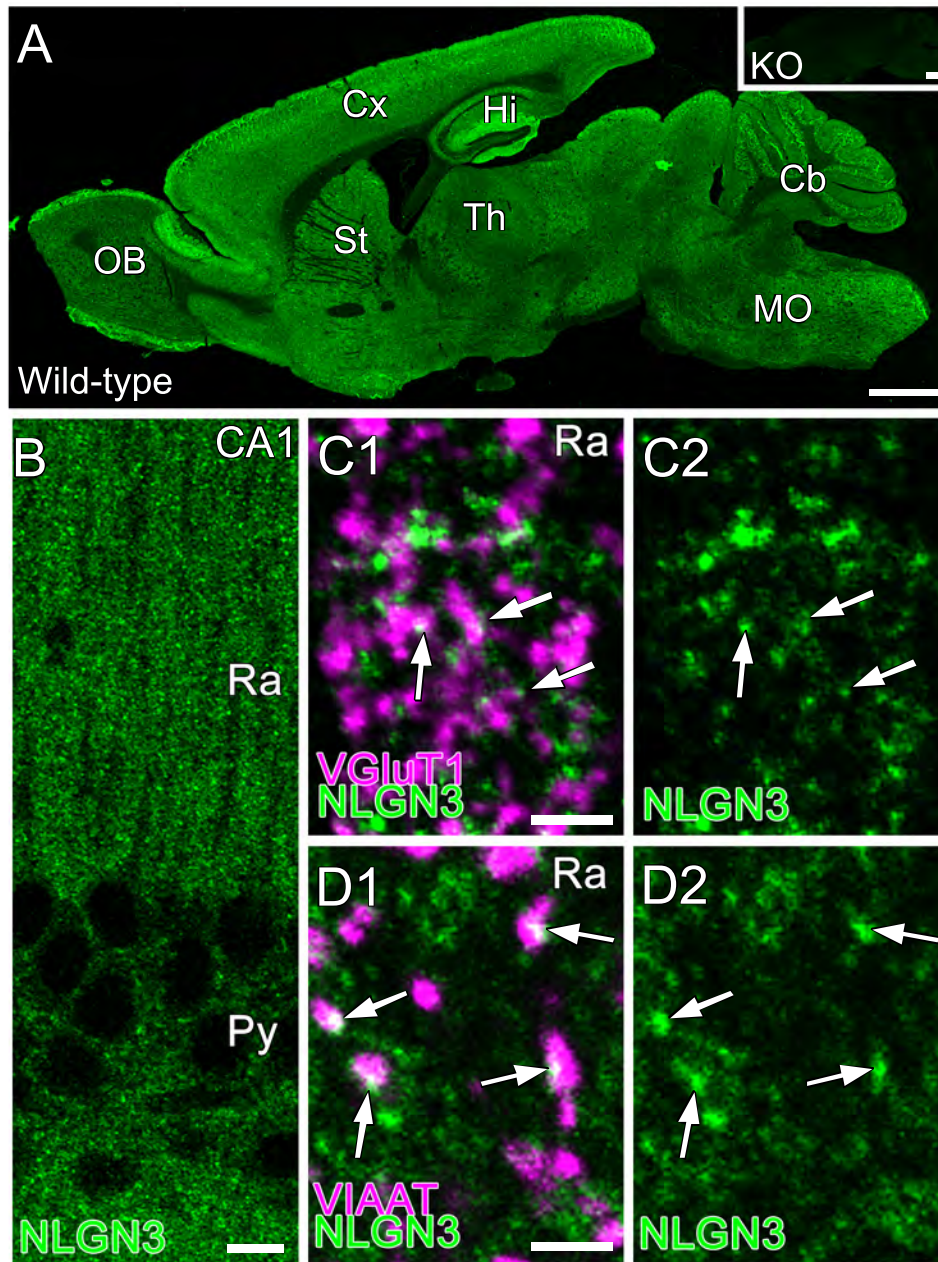


**Figure 2.** Subcellular localization of NLGN3 in the hippocampal CA1 area. **A.** Immunohistochemical staining for NLGN3 in whole brains of eight-week-old wild-type and *Nlgn3*-knockout mice (*Nlgn3*-KO, inset). **B.** Immunohistochemical staining for NLGN3 in the hippocampal CA1 area. **C, D.** Double immunohistochemical staining for NLGN3 (green) and VGLUT1 (**C**, magenta) or VIAAT (**D**, magenta) in the stratum radiatum of the hippocampal CA1 area. Cb, cerebellum; Cx, cortex; Hi, hippocampus; MO, medulla oblongata; OB, olfactory bulb; Py, stratum pyramidale; Ra, stratum radiatum; St, striatum; Th, thalamus. Scale bars: 1 mm (**A**), 10  $\mu$ m (**B**), 2  $\mu$ m (**C, D**).

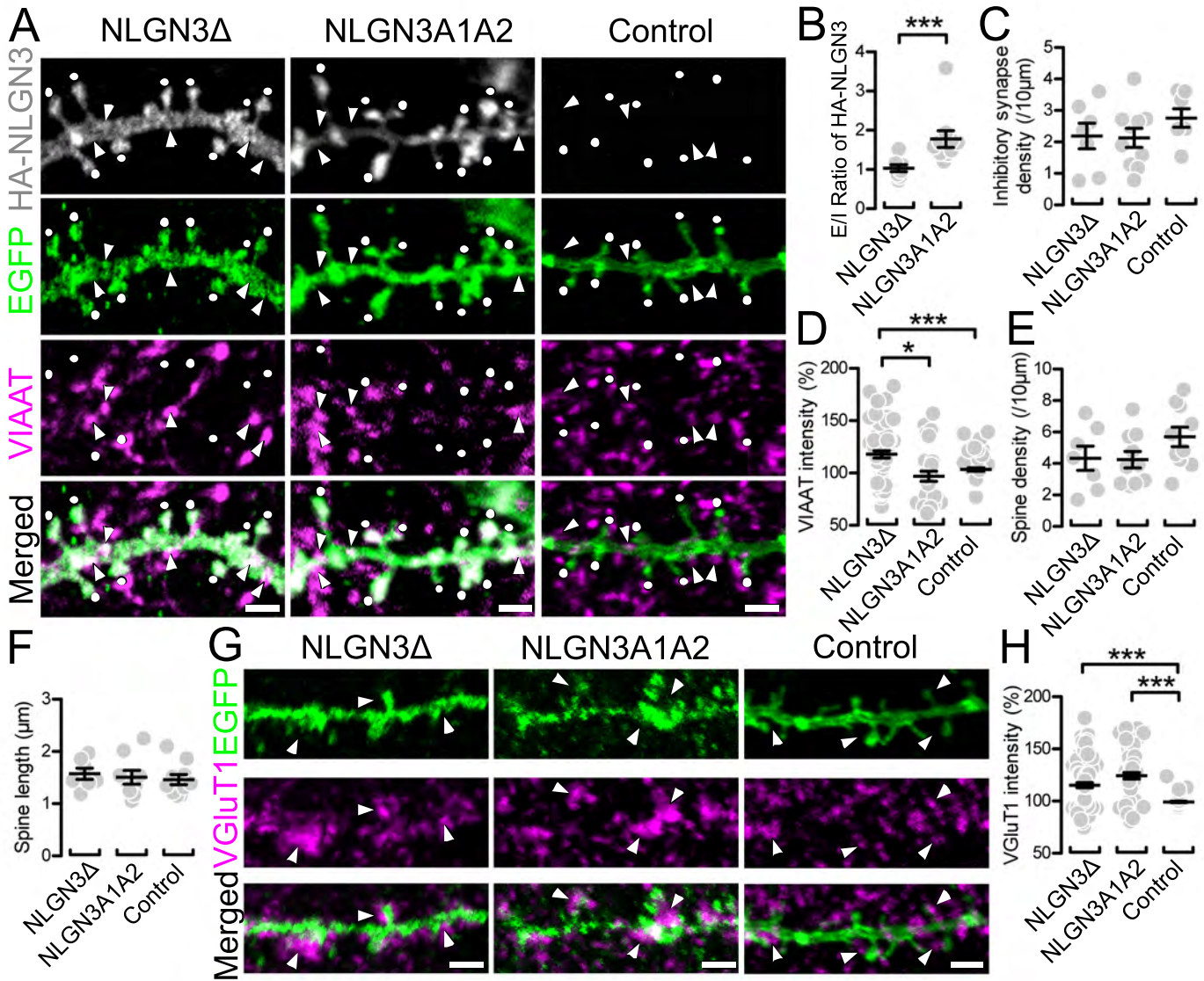


**Figure 3.** Synaptic targeting of NLGN3 splice isoforms in CA1 pyramidal neurons. **A.** Maximum projection images of dendritic segments labeled for HA-NLGN3 (gray), EGFP (green) and VIAAT (magenta) in CA1 pyramidal cells overexpressing HA-NLGN3 $\Delta$  (left), A1A2 (middle), and EGFP control (right). White dots and arrows indicate EGFP<sup>+</sup> spines and VIAAT<sup>+</sup> inhibitory synapses, respectively. Scale bars: 2  $\mu$ m. **B-F.** Summary scatter plot showing the E/I ratio of HA signals (**B**), inhibitory synapse density (**C**), VIAAT intensity (**D**), spine density (**E**), and spine length (**F**) for individual dendritic segments of CA1 pyramidal cells overexpressing HA-NLGN3 $\Delta$  (left, n = 7 dendrites), A1A2 (middle, n = 10), and control (right, n = 10). VIAAT intensity is normalized to the averaged VIAAT intensity in neighboring inhibitory terminals on the same image. **G.** Maximum projection images of dendritic segments labeled for EGFP (green) and VGlut1 (magenta) in CA1 pyramidal cells overexpressing HA-NLGN3 $\Delta$  (left), A1A2 (middle), and control (right). Arrowheads indicate VGlut1-labeled terminals contacting transfected dendrites. **H.** Summary scatter plot showing VGlut1 intensity for individual dendritic segments of CA1 pyramidal cells overexpressing HA-NLGN3 $\Delta$  (left, n = 7 dendrites), A1A2 (middle, n = 6), and control (right, n = 7). VGlut1 intensity is normalized to the averaged VGlut1 intensity in neighboring excitatory terminals on the same image. Scale bars: 2  $\mu$ m. \*  $p < 0.05$ , \*\*\*  $p < 0.001$  (one-way ANOVA followed by Sidak's multiple comparisons test or U-test).

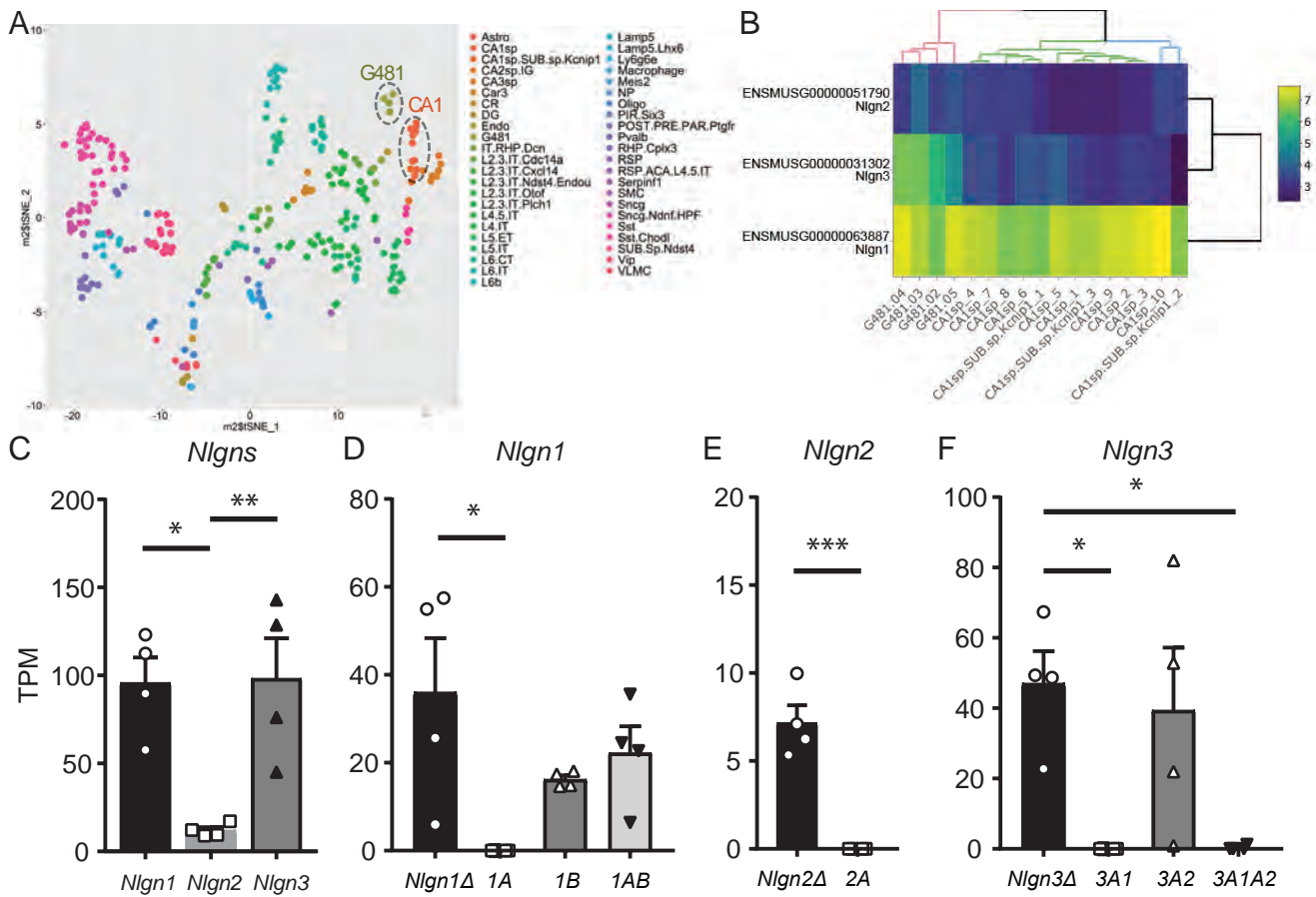


**Figure 4.** Endogenous *Nlgn* expression in hippocampal CA1 pyramidal neurons. **A.** Single-cell t-SNE plot of four single-cells (G481.02, .03, .04 and .05) and Allen Brain Atlas single-cells. **B.** Heat map of *Nlgn* gene expression in hippocampal CA1 primary neurons. A hierarchical clustering demonstrated a segregation of G481 cells from adult CA1 pyramidal neurons for *Nlgn3*, potentially due to relatively higher expression of *Nlgn3* in G481 cells. Scale bar shows log<sub>2</sub>+1 transformed TPM values. **C.** Summary bar graph of *Nlgn* gene (*Nlgn1*, 2 and 3) expression. **D-F.** Summary graphs of splice isoforms of *Nlgn1* (**D**), 2 (**E**) and 3 (**F**). \* p < 0.05, one-way ANOVA followed by Sidak's multiple comparisons test or U-test, n = 4.

**Neurologin3 splice isoforms shape inhibitory synaptic function in the mouse  
hippocampus**

Motokazu Uchigashima, Ming Leung, Takuya Watanabe, Amy Cheung, Timmy Le, Sabine Pallat, Alexandre Luis Marques Dinis, Masahiko Watanabe, Yuka Imamura Kawasawa and Kensuke Futai

*J. Biol. Chem.* published online May 7, 2020

---

Access the most updated version of this article at doi: [10.1074/jbc.AC120.012571](https://doi.org/10.1074/jbc.AC120.012571)

Alerts:

- [When this article is cited](#)
- [When a correction for this article is posted](#)

[Click here](#) to choose from all of JBC's e-mail alerts

## Supporting Experimental Procedure

### Neuroigin3 splice isoforms shape inhibitory synaptic function in the mouse hippocampus

Motokazu Uchigashima<sup>1,2,5</sup>, Ming Leung<sup>3,5</sup>, Takuya Watanabe<sup>1,5</sup>, Amy Cheung<sup>1</sup>, Timmy Le<sup>1</sup>, Sabine Pallat<sup>1</sup>, Alexandre Luis Marques Dinis<sup>1</sup>, Masahiko Watanabe<sup>2</sup>, Yuka Imamura Kawasawa<sup>3,4\*</sup> and Kensuke Futai<sup>1\*</sup>

<sup>1</sup>Brudnick Neuropsychiatric Research Institute, Department of Neurobiology, University of Massachusetts Medical School, 364 Plantation Street, LRB-706 Worcester, MA 01605-2324, USA  
<sup>2</sup>Department of Anatomy, Hokkaido University Graduate School of Medicine, Sapporo, Hokkaido 060-8638, Japan

<sup>3</sup>Department of Biochemistry and Molecular Biology and Institute for Personalized Medicine, Pennsylvania State University College of Medicine, 500 University Drive, Hershey, Pennsylvania 17033, USA

<sup>4</sup>Department of Pharmacology Pennsylvania State University College of Medicine, 500 University Drive, Hershey, Pennsylvania 17033, USA

<sup>5</sup>These authors contributed equally

\*Corresponding authors:

Yuka Imamura Kawasawa

E-mail: [yimamura@pennstatehealth.psu.edu](mailto:yimamura@pennstatehealth.psu.edu)

Kensuke Futai

E-mail: [Kensuke.Futai@umassmed.edu](mailto:Kensuke.Futai@umassmed.edu)



**Plasmid constructs:** The expression vector for HA-tagged mouse *Nlgn3A* has been reported previously (11). Three HA-tagged *Nlgn3* splice variants, *Nlgn3A1*, *Nlgn3A2* and *Nlgn3A1A2*, were cloned to pCAG vector using a PCR-based method.

**Single-cell sequencing and analysis:** *Single-Cell RNA Extraction:* The whole cell patch-clamp technique was used to harvest single cell cytosol (6). Briefly, glass electrodes (1.5 – 2.0 MΩ) were filled with DEPC-treated internal solution containing (in mM): 140 K-methanesulfonate, 0.2 EGTA, 2 MgCl<sub>2</sub> and 10 HEPES, pH-adjusted to 7.3 with KOH. RNase inhibitor (1 U/μl, Ambion) was included in the internal solution. Immediately after establishing whole-cell mode, the cytosol of the recorded cell was aspirated into the patch pipette and immediately expelled into an RNase-free 0.5-ml tube (Ambion). *Library Preparation and mRNA Sequencing:* The cDNA libraries were prepared using a SMART-Seq® HT Kit (TAKARA Bio) and a Nextera XT DNA Library Prep Kit (Illumina) as per the manufacturers' instructions. Unique barcode sequences were incorporated into the adaptors for multiplexed high-throughput sequencing. The final product was assessed for its size distribution and concentration using a BioAnalyzer High Sensitivity DNA Kit (Agilent Technologies). The libraries were pooled and diluted to 3 nM using 10 mM Tris-HCl (pH 8.5) and then denatured using the Illumina protocol. The denatured libraries were loaded onto an S1 flow cell on an Illumina NovaSeq 6000 (Illumina) and run for 2 x 50 cycles according to the manufacturer's instructions. De-multiplexed sequencing reads were generated using Illumina bcl2fastq (version 2.18.0.12) allowing no mismatches in the index read. *Data Analysis:* BBDuk (<https://jgi.doe.gov/data-and-tools/bbtools/bb-tools-user-guide/bbdduk-guide/>) was used to trim/filter low quality sequences using the “qtrim=lr trimq=10 maq=10” option. Next, alignment of the filtered reads to the mouse reference genome (GRCm38) was performed using HISAT2 (version 2.1.0) (<https://genomebiology.biomedcentral.com/articles/10.1186/gb-2013-14-4-r36>) applying --no-mixed and --no-discordant options. Read counts were calculated using HTSeq (<http://bioinformatics.oxfordjournals.org/content/31/2/166>) by supplementing Ensembl gene annotation (GRCm38.78). Gene expression values were calculated as transcripts per million (TPM) using custom R scripts. Genes with no detected TPM in all samples were filtered out. The log<sub>2</sub>+1 transformed TPM values were combined with “Cell Diversity in the Mouse Cortex and Hippocampus RNA-Seq Data” from the Allen Institute for Brain Science ([https://portal.brain-map.org/atlas-and-data/rnaseq#Mouse\\_Cortex\\_and\\_Hip](https://portal.brain-map.org/atlas-and-data/rnaseq#Mouse_Cortex_and_Hip)) where large-scale single-cell RNA-seq data were collected from the adult mouse brain. RNA sequencing data were generated from single cells isolated from >20 areas of the mouse cortex and hippocampus, including ACA, AI, AUD, CA, CLA, CLA:EPd, ENTI, ENTm, GU;VISC;AIP, HIP, MOp, MOs, ORB, PAR;POST;PRE, PL;ILA, PTLp, RSP, RSPv, SSp, SSs, SSs;GU, SSs;GU;VISC, SUB;ProS, TEa;PERI;ECT, VISal;VISl;VISli, VISam;VISpm, VISp and VISpl;VISpor (abbreviations for each cell type match those found in the Allen Mouse Brain Atlas (<https://portal.brain-map.org/explore/classes/nomenclature>)). The provided table of median expression values for each gene in each cell type cluster was merged with our data, and a tSNE plot was generated using Rtsne R package (29). For splice isoform quantification, kallisto (30) was used by supplementing the transcript fasta file (Mus\_musculus.GRCm38.cdna.all.fa), which was manually modified to include six *Nlgn* splice isoforms (*Nlgn1A\_XM\_006535423.3*, *1B\_XM\_006535424.4*, *2A\_XM\_006532902.4*, *2A\_XM\_006532903.3*, *3A* and *3A1*) that were not annotated by the Mus\_musculus.GRCm38.cdna.all.fa dataset. The manually curated transcript sequences are provided in **Fig. S2**.

**Single-cell semi-quantitative RT-PCR (semi-RT-qPCR):** The single cell cytosol was harvested using the whole cell patch-clamp technique as described earlier and the cDNA was prepared using a SMART-Seq® HT Kit (TAKARA Bio) as per the manufacturers' instructions. The semi-quantitative PCR was performed using GoTaq Master Mix (Promega) and primers for *Nlgn1*, *Nlgn2* and *Nlgn3* splice variants are: NL1, 5'-CTATACTTAAACATCTATGTCCCA -3' and 5'-GCTGGAAAGGGCTGTTCCACTCTGA -3'; NL2A, 5'-CTGTACCTCAACCTCTAC GTGCC -3' and 5'-ATAGGCAGCCAGGACTGAGCCGTC -3'; NL3A1A2, 5'-CTCTATCTGAATGTGTATGTGCC -3' and 5'-GTAAGTCAAGAACACTGCCATCAAT -3'. The expected size of *Nlgn* splice isoforms are: *Nlgn1A*

(420 bp), *Nlgn1A* (480), *Nlgn1B* (447), *Nlgn1AB* (507), *Nlgn2A* (138), *Nlgn2A* (189), *Nlgn3A* (138), *Nlgn3A1* (198), *Nlgn3A2* (198), *Nlgn3A1A2* (258). The PCR product was assessed for its size and concentration using a BioAnalyzer High Sensitivity DNA Kit (Agilent Technologies).

**Analysis of immunocytochemistry images:** For quantification of HA signals, the peak signal intensity was measured at a pair of excitatory and inhibitory synapses on dendritic segments which were identified as a EGFP-labeled spine and its neighboring VIAAT-labeled inhibitory terminal, respectively. E-I balance ratio was calculated by dividing the peak signal intensity at excitatory synapses by that at inhibitory synapses. The background signal was determined as the mean signal intensity in EGFP-unlabeled regions, and then subtracted from the raw value to obtain the peak signal intensity. To assess the labeling intensity for VIAAT, the contour of VIAAT+ terminals was determined using binary images for the VIAAT channel. The mean intensity was measured in VIAAT+ terminals contacting and not contacting EGFP-labeled dendrites, and then normalized with the average intensity for VIAAT+ terminals which were not in contact with EGFP-labeled dendrites on the same image. This measurement was also applied to the labeling intensity for VGluT1. To assess the density of excitatory and inhibitory synapses, the number of spines and VIAAT+ inhibitory synapses were counted on individual dendritic segments, respectively. The mean length of dendritic segments was  $19.7 \pm 3.8$ ,  $21 \pm 2.1$ , and  $27.7 \mu\text{m}$  for CA1 pyramidal cells overexpressing HA-NLGN3 $\Delta$ , 3A1A2, and EGFP control, respectively.

**Electrophysiology:** The extracellular solution consisted of (in mM): 119 NaCl, 2.5 KCl, 4 CaCl<sub>2</sub>, 4 MgCl<sub>2</sub>, 26 NaHCO<sub>3</sub>, 1 NaH<sub>2</sub>PO<sub>4</sub>, 11 glucose and 0.01 2-chloroadenosine (Sigma) gassed with 5% CO<sub>2</sub> and 95% O<sub>2</sub>, pH of 7.4. Thick-walled borosilicate glass pipettes were pulled to a resistance of 2.5 – 4.0 M $\Omega$ . Whole-cell voltage-clamp recordings were performed with internal solution containing (in mM): 115 cesium methanesulfonate, 20 CsCl, 10 HEPES, 2.5 MgCl<sub>2</sub>, 4 ATP disodium salt, 0.4 guanosine triphosphate trisodium salt, 10 sodium phosphocreatine and 0.6 EGTA, at pH 7.25 adjusted with CsOH. For current-clamp recordings, cesium was replaced by potassium. All experiments and the analysis of data were performed in a blind manner. Recordings were performed using a MultiClamp 700B amplifier and Digidata 1440, digitized at 10 kHz and filtered at 4 kHz using a low-pass filter. Data were acquired and analyzed using pClamp (Molecular Devices).

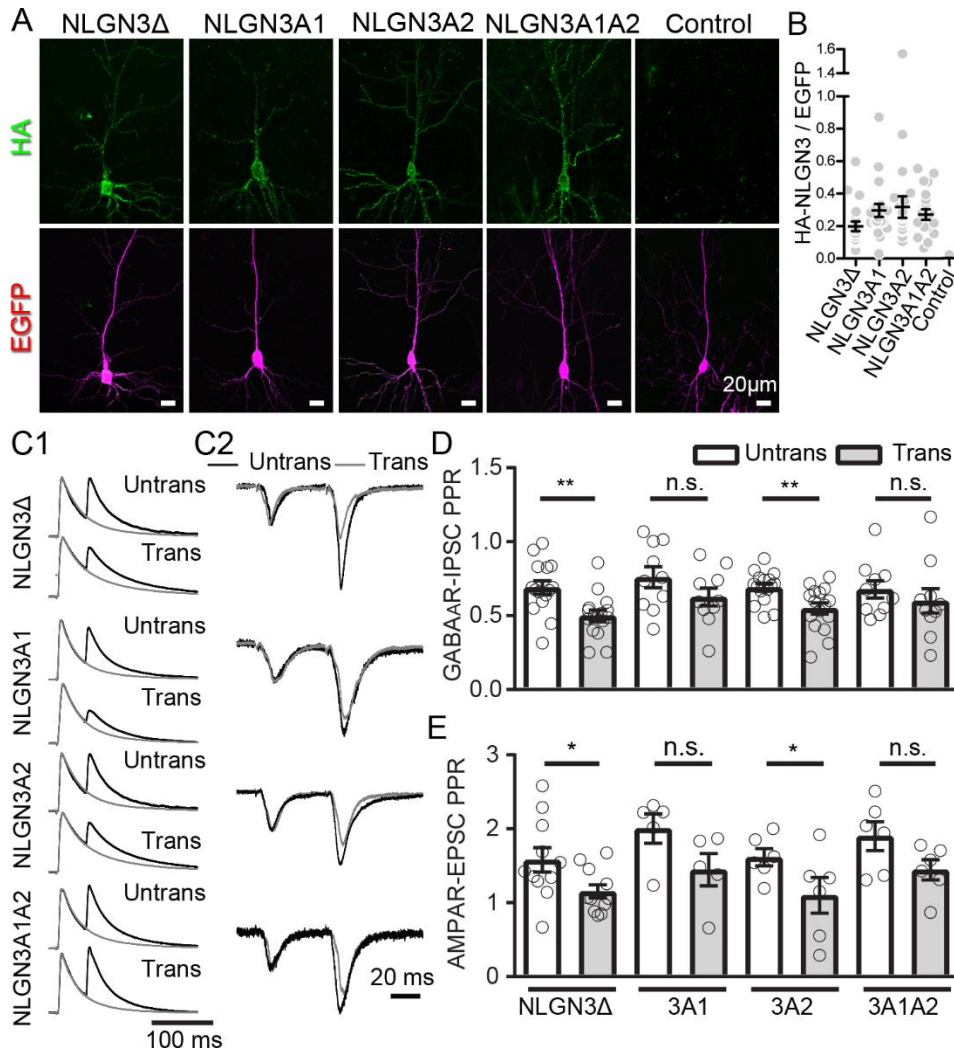


**Figure S1.** NLGN3 splice isoforms differentially regulate presynaptic release probability. Effect of NLGN3 splice isoform overexpression on gross morphology and PPR in hippocampal CA1 pyramidal cells. **A.** Low magnification images of entire neurons labeled with HA-NLGN3 and EGFP in CA1 pyramidal cells. **B.** Summary scatter plot showing the normalized intensity of HA signals in the cell bodies indicates that all four splice isoforms are equally overexpressed. **C.** Normalized sample traces of PPR of GABA<sub>A</sub>R-IPSC (left, **C1**) and AMPAR-EPSC (right, **C2**). IPSCs and EPSCs are normalized to the first amplitude. Because the first GABA<sub>A</sub>R-IPSC overlaps with the second IPSC, to accurately measure the amplitude of the second IPSC, we ‘cancelled’ the first IPSC by subtracting the traces receiving a single pulse (gray) from those receiving a paired pulse (black), both normalized to the first response. **D, E.** Summary of effect of NLGN3 transfection on IPSC- (**D**) and EPSC-PPR (**E**). Each bar represents the average of ratios obtained from multiple pairs of transfected and untransfected neighboring neurons. Number of cell pairs: NLGN3 $\Delta$  (GABA<sub>A</sub>R-IPSCs/AMPA-EPSCs: 15/11); NLGN3A1 (10/5); NLGN3A2 (15/6); NLGN3A1A2 (10/6). \*\*  $p < 0.01$ , \*  $p < 0.05$ , ns, not significant. Student’s t-test.

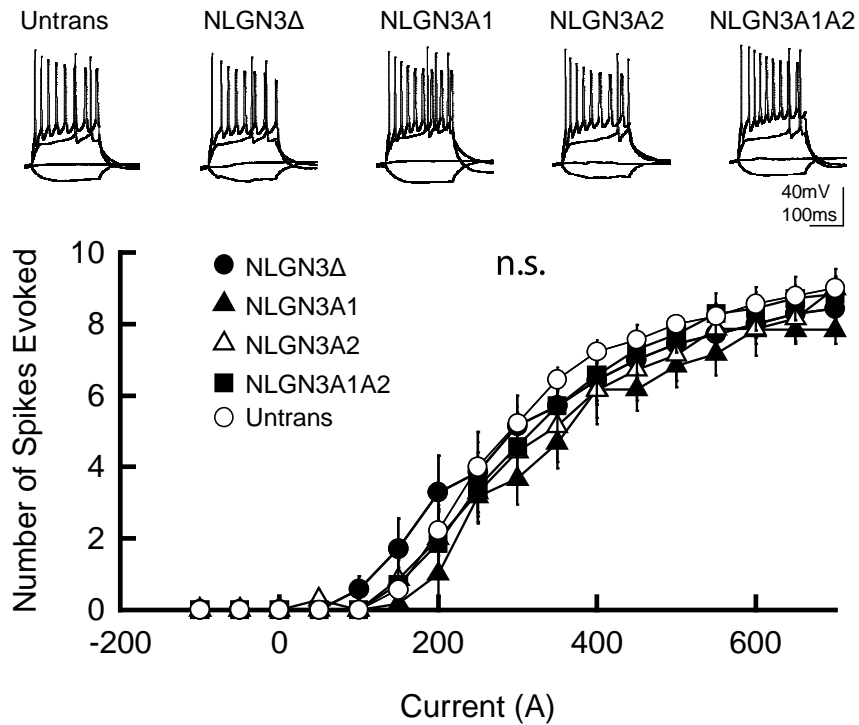


**Figure S2.** Membrane excitability is not altered by NLGN3 overexpression in CA1 pyramidal neurons. **Top.** Sample traces from untransfected and transfected CA1 pyramidal neurons in organotypic hippocampal slice cultures. The superimposed traces were elicited by current injections of -100, 0, 200 and 500 pA for 200 ms. **Bottom.** Summary graph of the frequency of action potentials in untransfected and transfected neurons. I-O relationship (number of spikes elicited vs. amount of current injection over a 200 ms duration) was plotted for untransfected and transfected neurons. Neurons were held at resting membrane potential (Rmv) and the I-O relationships were not significant between untransfected control and NLGN3 transfected neurons. Two-way ANOVA with *post hoc* Tukey. n.s.: not significant. Rmvs were not significant in five cell groups: untransfected,  $-58.9 \pm 0.63$ ; NLGN3Δ,  $-58.0 \pm 0.52$ ; NLGN3A1,  $-57.7 \pm 0.37$ ; NLGN3A2,  $-58.64 \pm 0.81$ ; NLGN3A1A2,  $-58.36 \pm 0.70$  mV. One-way ANOVA followed by Sidak's multiple comparisons test. Seven to nine cells from 2 mice were tested.

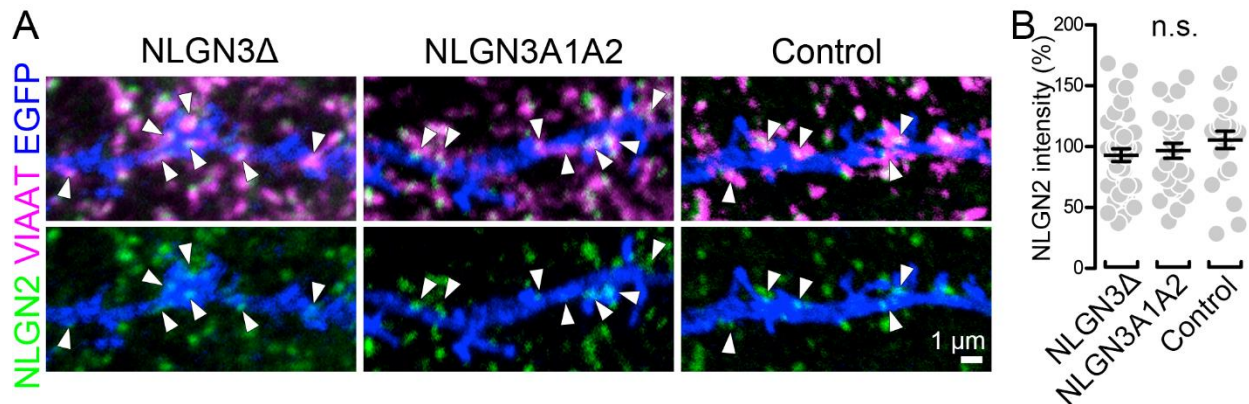


**Figure S3.** NLGN3 overexpression does not change synaptic targeting of NLGN2 in CA1 pyramidal neurons. **A.** Maximum projection images of dendritic segments labeled for NLGN2 (green), EGFP (blue) and VIAAT (magenta) in CA1 pyramidal cells overexpressing HA-NLGN3 $\Delta$  (left), A1A2 (middle) and EGFP control (right). White arrow heads indicate VIAAT+ and NLGN2+ inhibitory synapses in transfected neurons. **B.** Summary scatter plot showing the normalized NLGN2 signals for individual VIAAT+ inhibitory synapses on the dendritic segment of CA1 pyramidal cells overexpressing HA-NLGN3 $\Delta$  (left, n = 43 inhibitory synapses), A1A2 (middle, n = 27), and EGFP control (right, n = 23). Normalized NLGN2 intensity was obtained from neighboring VIAAT+ inhibitory synapses on the same image. n.s. not significant (one-way ANOVA followed by Sidak's multiple comparisons test).

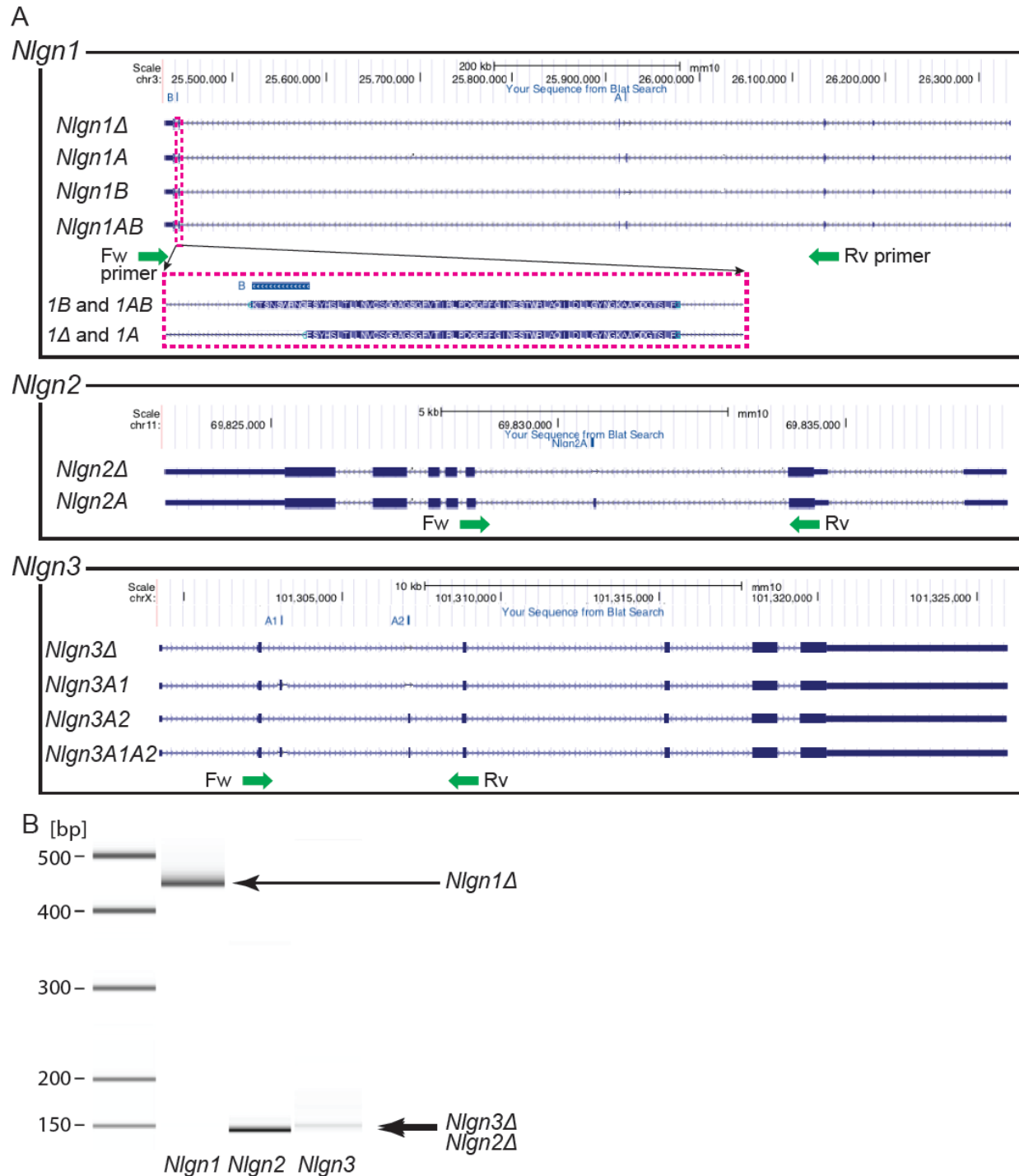


**Figure S4.** UCSC browser tracks of *Nlgn1*, 2 and 3, and semi-qPCR of hippocampal CA1 pyramidal neuron. **A.** 10 *Nlgn* transcripts and isoform-specific exons (A, B, *Nlgn2A*, A1 and A2; highlighted in blue) were manually curated. Green arrows depict locations of exon-specific PCR primers. **B.** Semi-quantitative RT-PCR of *Nlgn1*, *Nlgn2*, and *Nlgn3* in single-cell CA1 pyramidal neuron showed exclusive expression of  $\Delta$  isoforms (predicted amplicon sizes for *Nlgn1* $\Delta$ =420 bp, *Nlgn2* $\Delta$ =138 bp, and *Nlgn3* $\Delta$ =138 bp).